

# TEMPORAL DELAYS IN BLIND IDENTIFICATION OF PRIMARY SOMATOSENSORY CORTEX

MATTHEW T. SUTHERLAND<sup>1</sup>, JINGYU LIU<sup>2</sup>, AKAYSHA C. TANG<sup>1,3,4</sup>,

<sup>1</sup>Department of Psychology, <sup>2</sup>Department of Electrical and Computer Engineering, <sup>3</sup> Department of Neuroscience, <sup>4</sup> Department of Computer Science, University of New Mexico, Albuquerque, NM, 87131, USA  
E-MAIL: msuther@unm.edu, jingyu@unm.edu, akaysha@unm.edu

## Abstract:

Blind source separation (BSS) is an emerging statistical and data processing technique which aims to recover unobservable source signals from the observed mixtures. Second-order blind identification (SOBI) is one BSS algorithm that relies on stationary second-order statistics based on joint diagonalization of a set of covariance matrices. In simulations, the use of multiple covariance matrices computed with different time delays,  $\tau$ s, was beneficial for source separation, particularly when the underlying sources had highly overlapping spectra. Given the spectral overlap between actual brain sources, we experimented with different sets of temporal delays to empirically determine their effects on the isolation of electrical signals arising from a temporally and spatially well characterized brain location, the primary somatosensory cortex (SI). Using EEG data collected during median nerve stimulation, we found that the successful isolation of left and right SI activity required the use of a range of time delays and that the best separation was observed when the largest range of  $\tau$ s from 1 up to 300 ms was used.

## Keywords:

Blind source separation (BSS), Second-order blind identification (SOBI), electroencephalography (EEG), primary somatosensory cortex (SI)

## 1. Introduction

Electroencephalographic (EEG) signals are mixtures of electrical activity recorded by an array of electrodes at the scalp. These mixtures include electrical signals arising from several regions of the brain as well as various artifacts related to muscle activity, eye-movement, blinking, line noise and others. Thus, inferring from the EEG, the location of an electrical source and its corresponding time course of activation has been difficult. Blind source separation (BSS) algorithms have been increasingly used to recover underlying sources of activation from EEG [1-6] and magnetoencephalographic (MEG) data [7-13].

Second-order blind identification (SOBI) [14-16] is one such BSS algorithm, and uses second order statistics based on a set of covariance matrices computed with varying time delays,  $\tau$ s. The number and range of time delays specified for computing these covariance matrices affects the quality of source separation. Previously simulated data was used to show that the use of multiple time delays improves SOBI source separation [16,17]. This was particularly so when there was high spectral overlap between sources [16]. Because electrical activity generated by neuronal populations within different brain regions have highly overlapping spectra, particularly in the 8-12 Hz frequency band, the appropriate selection of  $\tau$  values and ranges is critical for the source separation of neuronal activity from EEG or MEG data.

Given the importance of these time delay parameters for source separation, it is surprising that of the studies applying SOBI to MEG or EEG data [6,9,10,11,12,13] only one specified the range of  $\tau$ s used [12]. The present literature offers little with regard to what effect the values/ranges of selected  $\tau$ s may have on source separation. Furthermore, the quality of source separation from actual EEG or MEG data has not yet been evaluated when different time delays are used. In the present study, we evaluated the effect of different  $\tau$  ranges on the separation quality of actual EEG data. We choose to evaluate this effect using the well characterized activation of primary somatosensory cortex (SI) by median nerve stimulation.

The paper is organized as follows: Section 2 describes the EEG data used to evaluate the selected temporal delays; Section 3 describes the SOBI algorithm; Section 4 presents the SOBI-recovered SI sources; Section 5 shows separation results for the SI sources as a function of the temporal delays chosen; and Section 6 summarizes the key results.

## 2. Stimuli and EEG data

SI activation by median nerve stimulation has been well characterized both spatially and temporally and is therefore the electrical source generator we have chosen to

assess source separation quality. Median nerve stimulation is known to activate SI in the hemisphere contralateral to stimulation with the earliest response around 20ms after stimulation. The spatial origin of such activation is the posterior bank of the central sulcus.

Unilateral (L: left; R: right) and bilateral (B) stimulations were delivered intermixed and pseudo-randomly. This stimulation protocol was used to generate temporally overlapping activations in both hemispheres, thus providing a challenge for the decomposition of separate left and right SI sources. Stimulations were constant current square-wave pulses (duration: 0.25ms) delivered transcutaneously at the wrist. Stimulation intensity was adjusted slightly below motor threshold, i.e. not producing movement of the thumb (range: 4.5-8.5 mA; *mean* = 6.5 mA). The strength and location of stimulation was adjusted to produce subjectively equal sensations in the left and right hands. Subjects were instructed to keep their eyes closed for the duration of the experiment and no behavioral responses were required.

We collected EEG data from four right-handed subjects (2 males). Continuous EEG (sampling rate: 1000 Hz; bandpass filter: 0.1-200 Hz; duration: < 20 min) was recorded in an electrically shielded room with a 128-channel EEG system (SymAmps, Neuroscan, El Paso, TX) using tin electrodes mounted in a custom made cap (ElectroCap International, Eaton, OH). All channels were referenced to the nose and impedances were maintained below 10 k $\Omega$ . Electrode and landmark positions (nasion, left and right pre-auriculars) were digitized (Fastrack, Polhemus Inc., Colchester, VT) and used for subsequent source localization.

### 3. SOBI algorithm

Let  $\mathbf{x}(t)$  represent  $n$ -dimensional vectors which correspond to the  $n$  continuous time series from the  $n$  EEG channels. Then  $\mathbf{x}_i(t)$  corresponds to the continuous sensor readings from the  $i^{\text{th}}$  EEG channel. Because various underlying sources are summed via volume conduction to give rise to the scalp EEG, each of the  $\mathbf{x}_i(t)$  are assumed to be an instantaneous linear mixture of  $n$  unknown components or sources  $\mathbf{s}_i(t)$ , via the unknown mixing matrix  $\mathbf{A}$ .

$$\mathbf{x}(t) = \mathbf{A} \mathbf{s}(t) \quad (1)$$

SOBI uses the EEG measurement  $\mathbf{x}(t)$  and nothing else to generate an unmixing matrix  $\mathbf{W}$  that approximates  $\mathbf{A}^{-1}$ , and the vector of the estimated component values,  $\hat{\mathbf{s}}(t)$ ,

$$\hat{\mathbf{s}}(t) = \mathbf{W} \mathbf{x}(t), \quad (2)$$

where  $\hat{\mathbf{s}}(t)$  is the continuous time series of the components or recovered sources. Sensor space projections, which indicate the effect of a given component, in isolation, on all sensors are given by the estimated mixing matrix,

$$\hat{\mathbf{A}} = \mathbf{W}^{-1}. \quad (3)$$

The SOBI algorithm [14-16] proceeds in two stages. First, the sensor signals are zero-meaned and prespurred as follows:

$$\mathbf{y}(t) = \mathbf{B}(\mathbf{x}(t) - \langle \mathbf{x}(t) \rangle). \quad (4)$$

The angle brackets  $\langle \cdot \rangle$  denote an average over time, so the subtraction guarantees that  $\mathbf{y}$  will have a mean of zero. The matrix  $\mathbf{B}$  is chosen so that the correlation matrix of  $\mathbf{y}$ ,  $\langle \mathbf{y}(t)\mathbf{y}(t)^T \rangle$ , becomes the identity matrix. This is accomplished by moving to the PCA basis using,

$$\mathbf{B} = \text{diag}(\lambda_i^{-1/2})\mathbf{U}^T, \quad (5)$$

where  $\lambda_i$  are the eigenvalues of the correlation matrix,

$$\langle (\mathbf{x}(t) - \langle \mathbf{x}(t) \rangle) (\mathbf{x}(t) - \langle \mathbf{x}(t) \rangle)^T \rangle, \quad (6)$$

and  $\mathbf{U}$  is the matrix whose columns are the corresponding eigenvectors, that is, the ‘‘PCA components’’ of  $\mathbf{x}$ .

For the second stage, one constructs a set of matrices that, in the correct separated basis, should be diagonal. We chose a set of time delay values,  $\tau$ s to compute symmetrized correlation matrices between the signal  $\mathbf{y}(t)$  and a temporally shifted version of itself:

$$\mathbf{R}_\tau = \text{sym}(\langle \mathbf{y}(t)\mathbf{y}(t + \tau)^T \rangle). \quad (7)$$

Where,

$$\text{sym}(\mathbf{M}) = (\mathbf{M} + \mathbf{M}^T)/2, \quad (8)$$

is a function that takes an asymmetric matrix and returns a closely related symmetric one. This symmetrization discards some information, but the problem is already highly overconstrained, and the symmetrized matrices provide valid, albeit slightly weaker, constraints on the solution.

After calculating the  $\mathbf{R}_\tau$ , we look for a rotation  $\mathbf{V}$  that jointly diagonalizes all of them by minimizing,

$$\sum_{i \neq j} (\mathbf{V}^T \mathbf{R}_i \mathbf{V})_{ij}^2, \quad (9)$$

the sum of the squares of the off-diagonal entries of the matrix products  $\mathbf{V}^T \mathbf{R}_i \mathbf{V}$ , via an iterative process ([15]; using MATLAB code available on-line at <http://sig.enst.fr/~cardoso/>). The final estimate of the separation matrix is:

$$\mathbf{W} = \mathbf{V}^T \mathbf{B}, \quad (10)$$

which is used to derive the separated components as in Eq. 2.

Using Eq. 2 for the consequent estimated sources, and Eq. 3 for the corresponding estimated mixing matrix, the sensor signals resulting from just one of the components can be computed as,

$$\hat{\mathbf{x}}(t) = \hat{\mathbf{A}} \mathbf{D} \mathbf{w}(t) = \hat{\mathbf{A}} \mathbf{D} \hat{\mathbf{s}}(t), \quad (11)$$

where  $\mathbf{D}$  is a matrix of zeros except for ones on the diagonal entries corresponding to each component that is to be retained.

To localize a single component, one computes:

$$\hat{\mathbf{x}}^{(i)}(t) = \hat{\mathbf{s}}_i(t) \hat{\mathbf{a}}^{(i)} \quad (12)$$

where  $\hat{\mathbf{a}}^{(i)}$  is the  $i^{\text{th}}$  column of  $\hat{\mathbf{A}}$  and  $\hat{\mathbf{x}}^{(i)}(t)$  is the sensor image of source  $i$ . Because  $\hat{\mathbf{x}}^{(i)}(t)$  is at each point in time equal to the unchanging vector  $\hat{\mathbf{a}}^{(i)}$ , scaled by the time course of interest  $\hat{\mathbf{s}}_i(t)$ , dipole fitting algorithms will localize  $\hat{\mathbf{x}}^{(i)}(t)$  to the same location no matter what window in time is chosen.

#### 4. SOBI-recovered SI

Similar to previous applications of SOBI to MEG data [12,13], SOBI was applied to the unprocessed EEG (sensor) data without the standard steps of epoching, artifact rejection, baseline correction, filtering, removal of bad channels or signal averaging. The 128-channel sensor data was decomposed into 128 SOBI-recovered sources or components, each of which had a time course of activation and an associated sensor space projection.

To identify the SOBI components corresponding to left and right SI activity, both spatial and temporal criteria were used. Temporally, event-triggered averages or somatosensory evoked potentials (SEPs) must have shown characteristic SI responses to contralateral median nerve stimulation and spatially, the scalp current source density (CSD) maps and the equivalent current dipole locations,

obtained using BESA 5.0 (Brain Electrical Source Analysis; MEGIS Software, Munich, Germany), must have been in the vicinity of the hand region of SI for

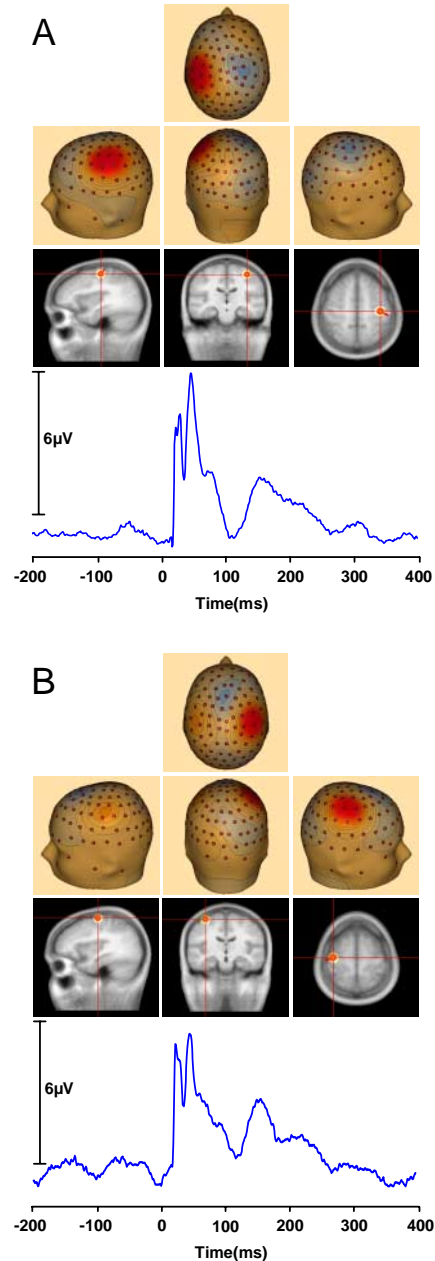


Figure 1. SOBI-recovered left SI (A) and right SI (B) from one subject. Top: scalp CSD maps. Middle: dipole locations. Bottom: contralateral SEPs.

components to be considered SI sources. Figure 1 shows an example of a SOBI-recovered left and right SI source.

## 5. Effects of temporal delays

Multiple temporal delays,  $\tau_s$ , can be specified for SOBI source separation. Previously, we have successfully used a set of  $\tau_s$  that ranged between delays from 1 up to 300ms (referred to as “standard set” from here after) for the source separation of EEG data collected during median nerve stimulation [18]. The spatial and temporal properties of such SI sources recovered using the “standard set” of temporal delays have been validated by comparing them with estimates obtained from converging imaging methods (i.e., fMRI, MEG, and high density EEG) [19]. The effect of different sets of  $\tau_s$  on the quality of source separation, using the following ranges (in ms), was assessed:

- “Standard set”, [1..300]:  
 $\tau \in \{1, 2, 3, 4, 5, 6, 7, 8, 9, 10, 12, 14, 16, 18, 20, 25, 30, 35, 40, 45, 50, 55, 60, 65, 70, 75, 80, 85, 90, 95, 100, 120, 140, 160, 180, 200, 220, 240, 260, 280, 300\}$
- Set 1, [1..2]:  
 $\tau \in \{1, 2\}$
- Set 2, [1..20]:  
 $\tau \in \{1, 2, 3, 4, 5, 6, 7, 8, 9, 10, 12, 14, 16, 18, 20\}$
- Set 3, [1..100]:  
 $\tau \in \{1, 2, 3, 4, 5, 6, 7, 8, 9, 10, 12, 14, 16, 18, 20, 25, 30, 35, 40, 45, 50, 55, 60, 65, 70, 75, 80, 85, 90, 95, 100\}$
- Set 4, [25..300]:  
 $\tau \in \{25, 30, 35, 40, 45, 50, 55, 60, 65, 70, 75, 80, 85, 90, 95, 100, 120, 140, 160, 180, 200, 220, 240, 260, 280, 300\}$ .

Separation results obtained using sets 1-4, which were subsets of the “standard set”, were compared with those using the “standard set” to evaluate the relative importance of different  $\tau$  ranges on separation quality. The SOBI-recovered left and right SI components (example shown in Fig. 1) were determined using the “standard set”. Set 1 was selected to evaluate whether left and right SIs could be isolated when temporal delays were virtually discarded. Results from sets 2-4 were compared to that from the “standard set” to evaluate the contribution of different ranges of delays.

SOBI’s success in “cleanly” isolating left and right SI activity from other sources (i.e., separation quality) was evaluated according to three criteria. First, the variance in the sensor space projections of the recovered sources

accounted for by *only* SI related dipoles should be as high as possible (i.e., the goodness of fit,  $g$  should be near 100%), indicating successful separation. Second, the number of dipoles needed, in addition to those corresponding to SI dipoles, to obtain a minimum of 95% goodness of fit for the entire model, should be zero after successful separation. Third, the distance of the SI dipole locations to the SI locations determined using the “standard set” should be small.

When using the “standard set” of  $\tau_s$ , SOBI-recovered left and right SIs were relatively “cleanly” separated from other sources as indicated by the lack of activation present at regions of the scalp other than over SI in the CSD maps (Fig 1AB: top). Across the four subjects (Table 1), the recovered SIs from the “standard set” displayed high goodness of fit values (SOBI-recovered left SI:  $97.6 \pm 0.9\%$ , right SI:  $97.3 \pm 0.4\%$ ) and no additional dipoles (0) were needed to adequately model the components. This indicated that when the “standard set” of  $\tau_s$  was used, SOBI adequately separated SI activations from other sources.

When the [1..2] set of  $\tau_s$  (Table 1) was used, that is, when temporal delays were nearly completely discarded,

Table 1.  $\tau$  ranges and source separation quality

		SOBI Recovered SI					
		Left			Right		
Tau Range	Subject	Distance to "Standard"	$g$	#additional dipoles	Distance to "Standard"	$g$	#additional dipoles
"Standard" [1..300]	1	0.0	95.1	0	0.0	98.1	0
	2	0.0	98.4	0	0.0	97.1	0
	3	0.0	97.6	0	0.0	97.7	0
	4	0.0	99.2	0	0.0	96.3	0
	Mean SEM	0.0	97.6	0.0	0.0	97.3	0.0
[1..2]	1	7.5	58.9	6	10.0	71.9	5
	2	12.6	81.3	4	5.2	83.2	2
	3	13.6	69.1	4	4.8	61.7	6
	4	16.4	76.3	7	29.7	48.8	6
	Mean SEM	12.5	71.4	5.3	12.4	66.4	4.8
[1..20]	1	3.5	96.3	0	2.0	96.3	0
	2	7.1	62.3	1	2.8	74.2	2
	3	4.1	98.8	0	3.5	95.3	0
	4	8.6	95.7	0	1.4	94.1	1
	Mean SEM	5.8	88.2	0.3	2.4	90.0	0.8
[1..100]	1	2.0	96.0	0	1.0	98.3	0
	2	4.1	99.1	0	5.5	71.6	2
	3	1.0	98.8	0	2.8	96.4	0
	4	2.8	98.8	0	3.7	93.7	1
	Mean SEM	2.5	98.2	0.0	3.3	90.0	0.8
[25..300]	1	3.6	94.6	1	3.6	98.4	0
	2	1.4	97.9	0	1.4	97.0	0
	3	3.0	86.2	1	8.4	98.4	0
	4	5.1	97.6	0	1.4	97.4	0
	Mean SEM	3.3	94.1	0.5	3.7	97.8	0.0
		0.8	2.7	0.3	1.6	0.4	0.0

dipole locations for the recovered SIs substantially differed from those estimated using the “standard set” (distance to standard: left  $12.5 \pm 1.9\text{mm}$ ; right  $12.4 \pm 5.9\text{mm}$ ). More importantly, the number of additional dipoles needed to adequately model the data (left:  $5.3 \pm 0.8$ ; right:  $4.8 \pm 0.5$ ) was the greatest among the five sets assessed and the amount of variance explained by the SI dipoles was the lowest (left:  $71.4 \pm 4.9\%$ ; right:  $66.4 \pm 7.3\%$ ) indicating that the SI sources were still mixed with other sources.

When the set of  $\tau$ s was increased up to 20 ms (i.e., set [1..20]; Table 1), the distance from the estimated dipole locations to those from the “standard set” decreased in comparison to when the [1..2] set was used (left:  $5.8 \pm 1.2\text{ mm}$ ; right:  $2.4 \pm 0.5\text{ mm}$ ). The amount of variance

accounted for by the dipoles corresponding to SI increased, reaching  $88.2 \pm 8.7\%$  and  $90.0 \pm 5.3\%$  for the recovered left and right SIs respectively. The number of noise dipoles required to model the observed component data was reduced to a maximum of 2 in comparison to a maximum of 7 in the case of  $\tau$ s in the range of [1..2].

Inclusion of greater temporal delays up to 100 ms (i.e., set [1..100]; Table 1) further decreased the distance from the estimated dipole locations to those from the “standard set” (left:  $2.5 \pm 0.7$ ; right:  $3.3 \pm 0.9$ ) and increased the amount of variance accounted for by dipoles that corresponded to SI (left:  $98.2 \pm 0.7\%$ ; right:  $90.0 \pm 6.2\%$ ). However, there were still two cases where additional dipoles were needed to account for at least 95% of the variance in the sensor space projections.

When only  $\tau$ s greater than 20 ms were used (i.e. set [25..300], excluding short delays; Table 1), the distance from the estimated dipole locations to those from the “standard set” were  $3.3 \pm 0.8\text{ mm}$  and  $3.7 \pm 1.6\text{ mm}$  for left and right SI respectively, similar to distances observed when using set [1..100]. The goodness of fit for the SI related dipoles was  $94.1 \pm 2.7\%$  and  $97.8 \pm 0.4\%$  for the recovered left and right SI sources respectively. There were two cases where additional dipoles were needed to adequately model the sensor space projections.

Figure 2 shows graphically the effect of different  $\tau$  ranges on the isolation of the SOBI-recovered left and right SIs. The CSD maps from the recovered sources clearly showed sensor activation over SI for each  $\tau$  range selected. However, only when a full range of  $\tau$ s ([1..300]) was used (top row), were the SI activations “cleanly” separated from other sources. In all other cases, additional sources of activations were observed (most visible in the posterior views).

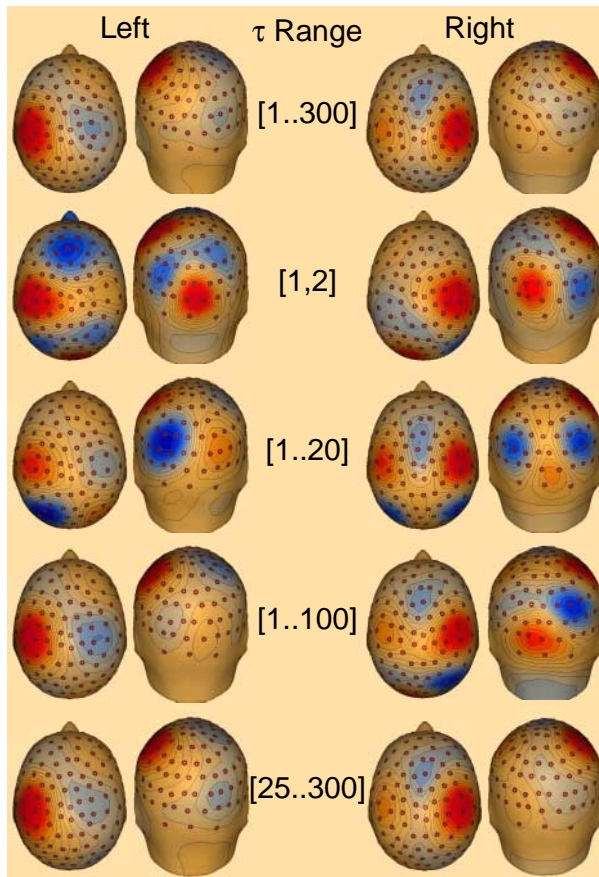


Figure 2. Recovered SI components using different  $\tau$  sets. Dorsal (left) and posterior (right) views of the CSD maps are shown from one subject. Sub-optimal separation is indicated by the presence of additional “spots” of activation at posterior scalp locations.

## 6. Conclusions

Although it is known that the number and range of time delays specified will affect the quality of SOBI source separation, how exactly the delays chosen affect the separation results of actual EEG data has not previously been investigated. In this paper, successful separation of SI activation by median nerve stimulation was used to evaluate SOBI separation quality. We found: (a) the best separation results were achieved when a full range of temporal delays, within the support of the autocorrelation function, was used; (b) when using a minimum number of temporal delays (i.e., [1..2]) SOBI failed to separate SI from other sources; (c) separation quality improved when larger ranges of time delays were used that included delays within 20 ms (i.e., sets [1..20] and [1..100]); (d) when temporal delays

less than 20 ms (i.e., set [25..300]) were excluded, the performance of SOBI source separation did not improve even though a relatively large range of time delays was used. To further understand the effects of temporal delays on SOBI separation of brain signals, it is important to conduct EEG domain specific simulations to systematically investigate how temporal delays can be selected to allow for the optimal separation of brain sources of interest.

### Acknowledgements

Supported by funding from the DARPA Augmented Cognition Program to A.C.T. We thank C.J. McKinney for technical assistance.

### References:

- [1] S. Makeig, T.-P. Jung, D. Ghahremani, A.J. Bell and T.J. Sejnowski, "Blind separation of auditory event-related brain responses into independent components, Proc. Natl. Acad. Sci. USA, Vol. 94, pp. 10979-10984, 1997.
- [2] S. Makeig, M. Westerfield, T.-P. Jung, J. Covington, J. Townsend, T.J. Sejnowski, and E. Courchesne, "Functionally independent components of the late positive event-related potential in a visual spatial attention task", J.Neurosci., Vol. 19, No. 7, pp. 2665-2680, 1999.
- [3] T.-P. Jung, S. Makeig, M. Westerfield, J. Townsend, E. Courchesne and T.J. Sejnowski, "Removal of eye activity artifacts from visual event-related potentials in normal and clinical subjects", Clin. Neurophysiol., Vol. 111, No. 10, pp.1745-1758, 2000.
- [4] T.-P. Jung, C. Humphries, T.-W. Lee, M.J. McKeown, V. Iragui, S. Makeig, and T.J. Sejnowski, "Removing electroencephalographic artifacts by blind source separation", Psychophysiol, Vol. 37, pp. 163-178, 2000.
- [5] R.N. Vigario, "Extraction of ocular artifacts from EEG using independent component analysis", Electroenceph and Clin. Neurophysiol., Vol. 103, pp. 395-404, 1997.
- [6] C.A. Joyce, I.F. Gorodnitsky, and M. Kutas, "Automatic removal of eye movement and blink artifacts from EEG data using blind component analysis", Psychophysiol., Vol. 41, No. 2, pp. 313-325, March 2004.
- [7] R. N. Vigario , J. Sarela, V. Jousmaki, M. Hamalainen, and E. Oja, "Independent component approach to the analysis of EEG and MEG recordings", IEEE Trans. Biomed. Eng., Vol. 47, pp. 589-593, 2000.
- [8] R. N. Vigario, and E. Oja, "Independence: A new criterion for the analysis of the electromagnetic fields in the global brain?", Neural Netw., Vol. 13, pp. 891-907, 2000.
- [9] G. Wubbeler, A. Ziehe, B.M. Mackert, K.R. Muller, L. Trahms, and G. Curio, "Independent component analysis of noninvasively recorded cortical magnetic DC-fields in humans", IEEE Trans. Biomed. Eng., Vol. 47, pp. 594-599, 2000.
- [10] A. Ziehe, K.R. Muller, G. Nolte, B.M. Mackert, and G. Curio, "Artifact reduction in magnetoneurography based on time-delayed second-order correlations", IEEE Trans. Biomed. Eng., Vol. 47, pp.75-87, 2000.
- [11] B.M. Mackert, G. Wubbeler, S. Leistner, L. Trahms, and G. Curio, "Non-invasive single-trial monitoring of human movement-related brain activation based on DC-magnetoencephalography", Neuroreport, Vol. 12, pp. 1689-1692, 2000.
- [12] A.C. Tang, B.A. Pearlmutter, N.A. Malaszenko, D.B. Phung, and B.C. Reeb, "Independent components of magnetoencephalography: localization", Neural Computation, Vol. 14, pp. 1827-1858, 2002.
- [13] A.C. Tang, B.A. Pearlmutter, N.A. Malaszenko, and D.D. Phung, "Independent components of magnetoencephalography: Single-trial response onset times", Neuroimage, Vol. 17, pp. 1773-1789, 2002.
- [14] A. Belouchrani, K.A. Meraim, J.-F. Cardoso, and E. Moulines, "Second-order blind separation of correlated sources", Proceedings of the International Conference on Digital Signal Processing, Cyprus, pp. 346-351, 1993.
- [15] J.-F. Cardoso, and A. Souloumiac, "Jacobi angles for simultaneous diagonalization", SIAM Journal of Matrix Analysis and Applications, Vol. 17, No.1, pp.161-164, Jan. 1996.
- [16] A. Belouchrani, K. Abed-Meraim, J.-F. Cardoso, E. Moulines, "A blind source separation technique using second-order statistics", IEEE Trans. On Signal Processing, Vol. 45, No. 2, pp. 434-444, Feb. 1997.
- [17] A. Ziehe, and K.-R. Muller, "TDSEP-An efficient algorithm for blind separation using time structure", Proceedings of the 8<sup>th</sup> ICANN, Berlin, Germany, pp. 775-780, 1998.
- [18] A. C. Tang, C.J. McKinney, and M.T. Sutherland, "Application of an ICA algorithm for the analysis of electroencephalographic data", Cognitive Neuroscience Society abstract, New York, April 2003.
- [19] A. C. Tang, M.T. Sutherland, and C.J. McKinney, "Validation of SOBI-recovered sources from high density EEG", *in submission*.